Journal of Structural Geology, Vol. 15, Nos 3–5, pp. 253 to 264, 1993
Printed in Great Britain

0191-8141/93 $06.00 + 0.00

Information from fold shapes

PETER J. HUDLESTON and LABAO LAN

Department of Geology and Geophysics, University of Minnesota, Minneapolis, MN 55455, U.S.A.

(*Received* 27 *December* 1991; *accepted in revised form* 10 *July* 1992)

Abstract—Folds contain information about the deformation rocks have undergone and the condition of the rocks during deformation. How much of this can we decipher? The geometrical characteristics of folds and the strain distribution within them are perhaps the key to unlocking this information. If the folded layers were originally planar, they reflect inhomogeneous deformation, but without additional originally planar or linear markers of other orientations, we cannot determine the state of strain. The strain in a parallel fold, for example, can be accommodated either by flexural slip or by tangential longitudinal strain, two quite different but geologically realistic strain distributions among an infinite number of possible ones. There are some constraints imposed by fold shapes on possible strain distributions. Fold asymmetry reflects, in most circumstances, sense of shear strain parallel to the general orientation of the folded layering. Problems may arise in shear zones with large strains and in foliated rocks in which kink bands develop at small strains. Information on the orientations of principal stresses cannot be obtained from folds, unless the strain is small and the mechanism of folding understood, as for kink bands, or unless the bulk flow is of constant vorticity, which is difficult to demonstrate.

The distribution of measured values of wavelength/thickness in a population of single-layer folds, together with measures of strain and estimates of amplification, can be used to estimate the viscosity ratio of the stiff layer to its matrix and the degree of non-linearity in the flow law, *if* effective power-law flow is assumed. Information on the rheological state of rocks at the time of folding can also be obtained from the pattern of curvature variation in individual single-layer folds, as demonstrated by the use of computer simulations of folding. Where applied, such methods indicate that the slow natural flow of rock involved in folding is mostly consistent with non-linear power-law rheology, as expected from the results of experimental rock deformation involving crystal-plastic deformation mechanisms.

INTRODUCTION

FOLDS in layered rocks have long attracted the attention of geologists, and this may be because they are so common and often striking in appearance in outcrop or on a map. They are highly variable in shape, as can be seen, for example, in Figs. 1 and 2 and in the many illustrations in Weiss (1972) and Ramsay & Huber (1987). This is perhaps not surprising considering the great variation in composition, and thus in physical properties, of rocks and the wide range of conditions under which folds form. We would, in fact, like to be able to utilize folds to obtain information about the deformation rocks have undergone and the condition of the rocks during deformation. To what extent can we do this? It is the purpose of this paper to summarize some of the earlier work that addresses this question and to present results of recent work we have been doing that may provide some information about rheological properties of rocks undergoing folding. We should state at the outset that there is non-uniqueness in interpreting fold shapes and strain patterns in terms of mechanisms and rock properties, and the best we can hope to do is to place limits on these. This is a useful exercise, nonetheless, because this approach is independent of laboratory methods of determining rheological properties of rocks, the results of which must be extrapolated over many orders of magnitude to predict behavior at geological strain rates. What is aimed at is mutual consistency among estimates of rheological properties from experimental results, from fabric and microfabric studies, and from fold shape and strain distribution. It is the latter that is the focus of this paper.

Methods of shape analysis

Many methods have been proposed for describing the shapes of folds, both qualitatively and quantitatively (e.g. Van Hise 1896, Busk 1929, Mertie 1959, Fleuty 1964, Ramsay 1967, chap. 7, Wilson 1967, Stabler 1968, Hudleston 1973, Ramsay & Huber 1987, sessions 15–17, Twiss 1988). Many schemes depend on the fact that there is a tendency for folds of a given set or generation to have sub-parallel axial surfaces and sub-parallel hinges. These properties, of course, are exploited in fold analysis using stereographic or equal-area projections. They are also utilized in the analysis of superimposed folds (Ramsay 1967, pp. 520–533, Thiessen 1986), and they are the reason why many interference patterns display such regularity.

Ramsay (1967, chap. 7) showed how it is useful to consider the shapes of folded *single-surfaces* separately from the shapes of folded *layers*. Various means of describing the shapes of single-surfaces have been proposed (e.g. Mertie 1959, Ramsay 1967, chap. 7, Stabler 1968, Hudleston 1973, Twiss 1988). Two of the most useful properties that can be readily measured or expressed qualitatively are the relative sizes of the 'hinge' and 'limb' regions of folds (see Ramsay 1967, p. 349) and the relative lengths of adjacent limbs, which is one measure of asymmetry. Chevron folds or kink bands (Fig. 2d) are examples of folds with narrow hinge zones

and long limbs. Folds that can be represented by circular arcs (parts of folds in Figs. 1b & d) have broad hinge zones and short limbs (Ramsay 1967, fig. 7-5). Quantitative representation of single-surface shape can be provided by harmonic analysis, which can be applied to segments of folds (Stabler 1968, Hudleston 1973), individual folds, or whole fold trains (Fletcher & Sherwin 1978) in establishing a spectrum of wavelengths. The nature of the variation in curvature around the arc of a fold characterizes any single-surface fold shape. A new method of utilizing curvature variations is presented later in this paper.

The shapes of individual folded layers are readily represented by plotting thickness as a function of 'dip' (measured with respect to the normal to the axial surface) on a section perpendicular to the hinge, and Ramsay's normalized orthogonal thickness (t'_α) vs dip (α) plot is perhaps the most familiar method employed (Ramsay 1967, p. 361). Dip isogons (Elliott 1965, Ramsay 1967, p. 363) provide a most useful means of linking single-surface and layer geometry. Ramsay's five fold classes (1A,1B,1C, 2 and 3), defined on the basis of isogon patterns, fall in distinct fields on a t'_α/α plot, and a representation based on isogons similar to a t'_α/α plot can be constructed (Hudleston 1973, fig. 2). Natural examples of folds of various shapes are shown in Figs. 1 and 2, including the familiar parallel (class 1B) fold (Figs. 1a and 2a), similar (class 2) fold (Fig. 2c), and more complex types (Figs. 1b–d and 2b).

STRAIN

If the layers were originally planar, their folded form in deformed rocks reflects inhomogeneous deformation. They may be considered one set of co-ordinates of a Lagrangian co-ordinate system. Without markers of the other (orthogonal) co-ordinates, we can say little about the state of strain. Ramsay (1967, figs. 7-54 and 7-63) has shown, for example, that the strain in a parallel (class 1B) fold can be accommodated either by flexural slip (or flexural flow) or by tangential longitudinal strain, two quite different strain distributions. These two possible strain distributions are shown in Fig. 3, with two additional ones, all geologically plausible. The strain patterns shown are those for an ideal fold shape formed by concentric circular arcs, which represent quite well the shape of a natural buckle fold in a limestone layer (Hudleston & Holst 1984). Note that initial markers perpendicular to the layering remain perpendicular after folding in *three* of the models, and thus only flexural slip could be distinguished from the other three on the basis of the orientations of such markers. To distinguish among the other three patterns requires information on strain magnitudes (or *spacing* of the originally orthogonal markers). The distinctions among the four models can be further appreciated by undeforming the grid of elements defining the ideal shapes in Fig. 3. This is done in Fig. 4. In the natural fold that these strain distributions were compared with, inner arc collapse with an initial homogeneous strain (Fig. 3d) provided the best match to the strain data (Hudleston & Holst 1984). There are in fact an infinite number of other possible strain patterns that match the same shape. One could, for example, impose an arbitrary initial homogeneous strain on the layer before folding by tangential longitudinal strain (Fig. 3a) or flexural flow (Fig. 3b). It should perhaps be pointed out that in a fold other than one represented by concentric circular arcs, the orthogonality between markers parallel and perpendicular to the layering cannot be strictly maintained for tangential longitudinal strain, whereas it can for inner arc collapse.

Although strain variations around folds may be of many different types (the patterns in Fig. 3, for example), there is often a symmetry of this pattern about the axial surface, which is typically perpendicular, or nearly so, to the bulk shortening direction of the deformation associated with the folding. Exceptions to this are provided by buckle folds in isolated competent layers oblique to the direction of bulk shortening (e.g. Treagus 1973, Manz & Wickham 1978), and the phenomenon of cleavage transection (Borradaile 1978, Johnson 1991), in which the symmetry of the strain pattern (as represented by cleavage orientation) about the axial surface is lost. The potential complexity of fold development in a progressive deformation of even the simplest kind (bulk coaxial strain, as described by Flinn 1962) is such that one might expect cleavage transection to be common.

Early studies of folds often ascribed simple mechanisms to certain common geometric patterns, and such studies provide an instructive example of the danger of interpreting folding mechanisms directly from fold shapes. The best example is that of similar (class 2) folds, in which every folded surface has the same shape (see Fig. 2c). These can be accounted for by heterogeneous simple shear of alternating sense parallel to the axial planes (Fig. 5a), as proposed, for example, by Carey (1962) and Billings (1972, p. 121), and such folds have been referred to as shear folds or slip folds. It seems that few similar (or more typically sub-similar) folds have actually formed by this mechanism, however, because of the mechanical difficulties of producing the required shear stresses of systematically changing magnitude and sense parallel to the axial planes of the folds, and because strain and fabric patterns in natural folds are not compatible with those predicted by the model (see Ramsay 1962, 1967 and Ramberg 1963 for discussion). Three other possible strain distributions within similar folds are shown in Fig. 5. The problematic reversal in sense of shear, but not variations in the amount of shear, can be eliminated by starting with a sufficiently oblique layer (Fig. 5c) (see also Ragan 1969), and a better match of predicted and observed strain patterns can be obtained if a uniform shortening is imposed in addition to the simple shear (Fig. 5b) or if the strain is entirely homogeneous and the fold results from the passive amplification of initial waviness in the layer (Fig. 5d). It should be pointed out that there is no distinction in final form between a fold formed as shown by coaxial strain in

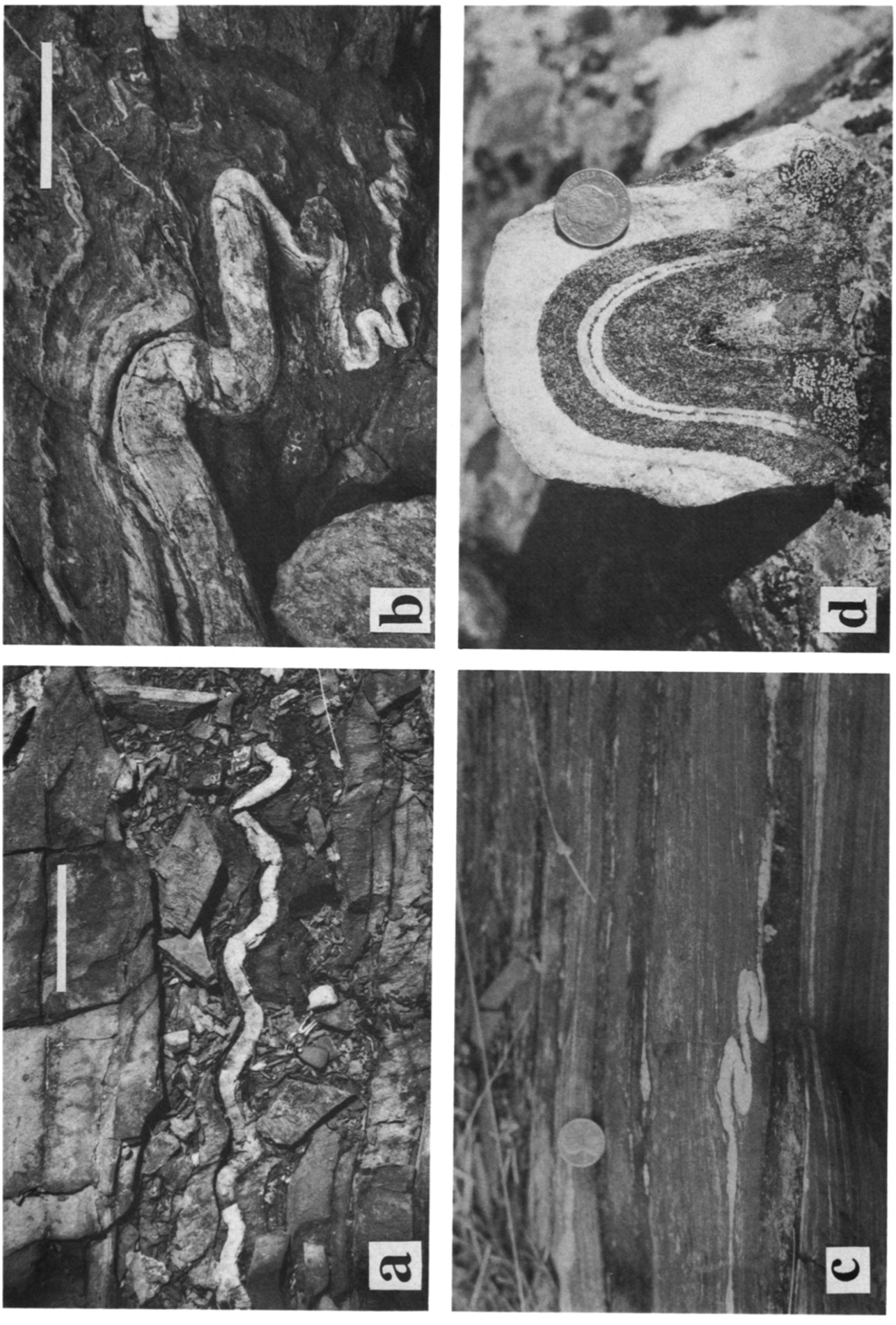

Fig. 1. Examples of natural folds to show geometric characteristics. (a) Buckled quartz vein in slates of the Hovin Group, near Trondheim, Norway. The folds are close to 1B (parallel) in shape. Scale bar is 20 cm. (b) Buckle folds in mylonitized pegmatite layer, Cap de Creus, Spain. Note the decrease in fold 'wavelength' as the layer thins to the right and the cusps developed on the inner arcs of the stiff layer. Scale bar is 40 cm. (c) Buckled quartz vein in ironstone and pelitic schist in a dextral shear zone, Geraldton, Ontario, Canada. The folds in the vein are class 1C ('flattened parallel folds'). Coin is 25 cm in diameter. (d) Double-hinged (outer arc) to single-hinged (inner arc) fold in amphibolite gneiss, Kebnekaise, Swedish Lappland. The inner dark (amphibole rich) layer is of fold class 1C. Coin is 25 cm in diameter.

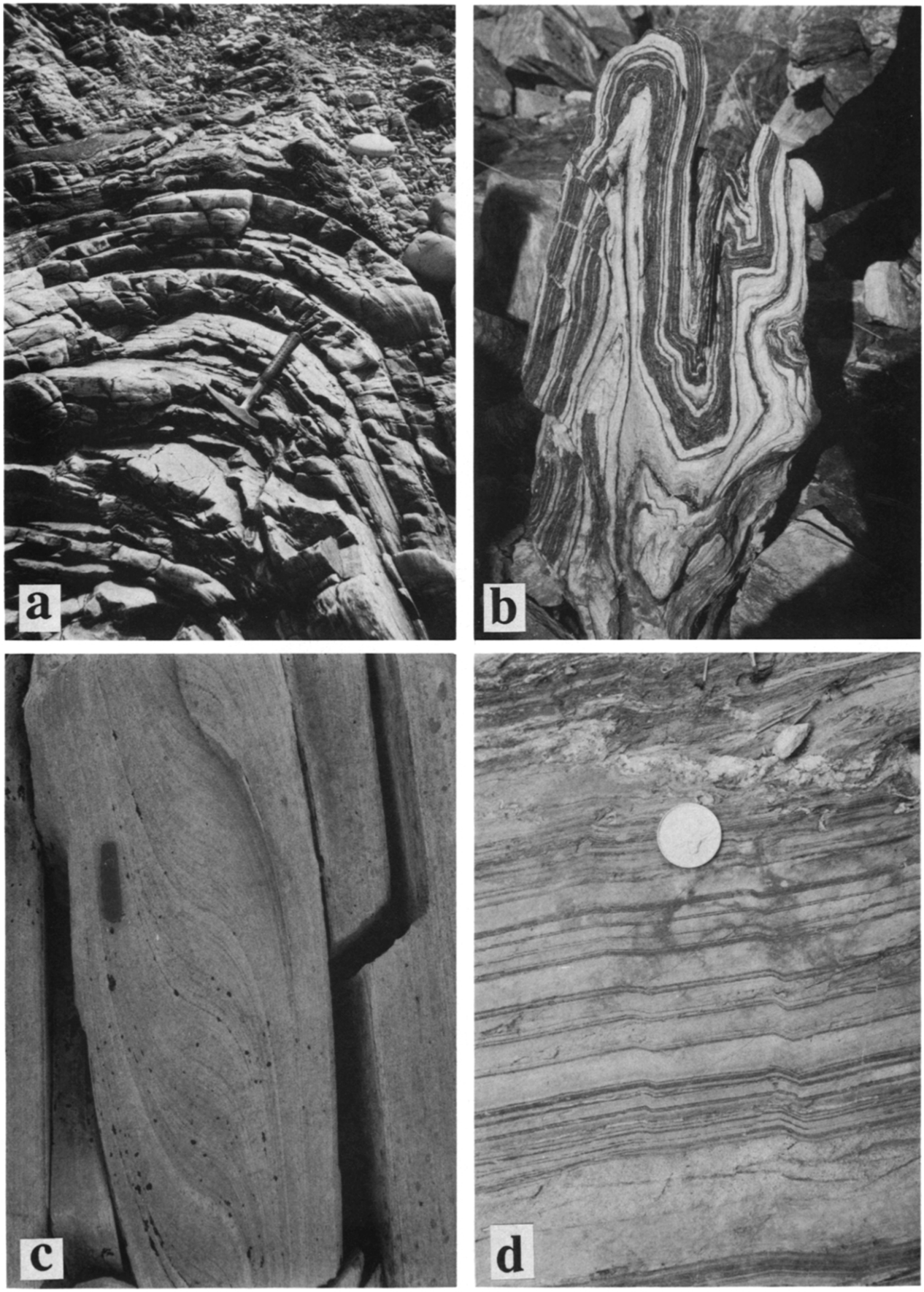

Fig. 2. Geometric characteristics of natural folds. (a) Parallel fold in Lewisian gneiss, Loch Hourn, Scotland. Hammer for scale. (b) Complex fold in amphibolitic Lewisian gneisses, Loch Hourn, Scotland. Note the non-parallel axial surface traces, and large and irregular variations in thickness of some layers. Pencil for scale. (c) Nearly perfect similar (class 2) fold in quartzite of the Saetra nappe, Trollheimen, Norway. Penknife is 10 cm long. (d) Kink bands in metasedimentary unit, near Jellicoe, Ontario, Canada. Coin is 25 cm in diameter.

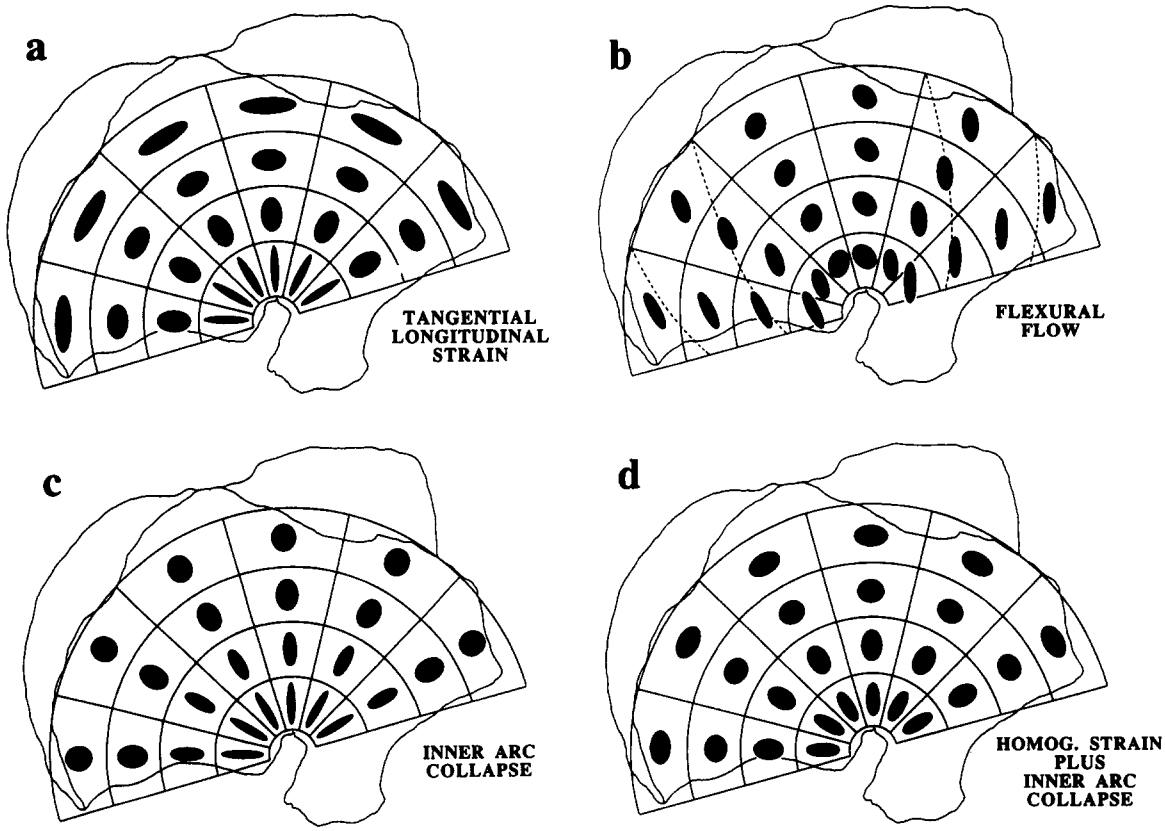

Fig. 3. Four possible strain distributions in a (parallel) fold represented by concentric circular arcs. The circular arcs and radii define segments of the fold in which the strain is represented by a black ellipse. Note that these arcs and radii only represent the deformed positions of original orthogonal co-ordinate lines in cases (a), (c) and (d), and that only in cases (b) and (c) is the original spacing of the concentric markers unchanged (see Fig. 4). (a) and (b) are plane strain and constant area. The dashed lines in (b) represent markers originally perpendicular to layering. See Hudleston & Holst (1984) for details of the analysis of this fold.

Fig. 5(d) and one formed by homogeneous simple shear, starting with an inclined wavy layer.

Rheological arguments have also been introduced to account for similar folding. Hobbs (1972) gave examples that show how the shapes of similar folds, formed in inhomogeneous simple shear of fluids, depend on the rheological properties of the fluids, and Cobbold (1976) demonstrated how perturbations in a planar anisotropic material can grow to produce similar folds (of chevron shape). Casey & Huggenberger (1985) simulated the development of similar folds numerically in anisotropic fluids or multilayers consisting of alternating isotropic viscosities, for any imposed bulk deformation. Strain patterns in the latter two cases will be similar to those shown in Figs. 5(b) & (d), and the 'problematic' reversal in sense of shear from limb to limb is provided by the buckling instability associated with the anisotropy.

If the viscosity contrast is high, competent layers will

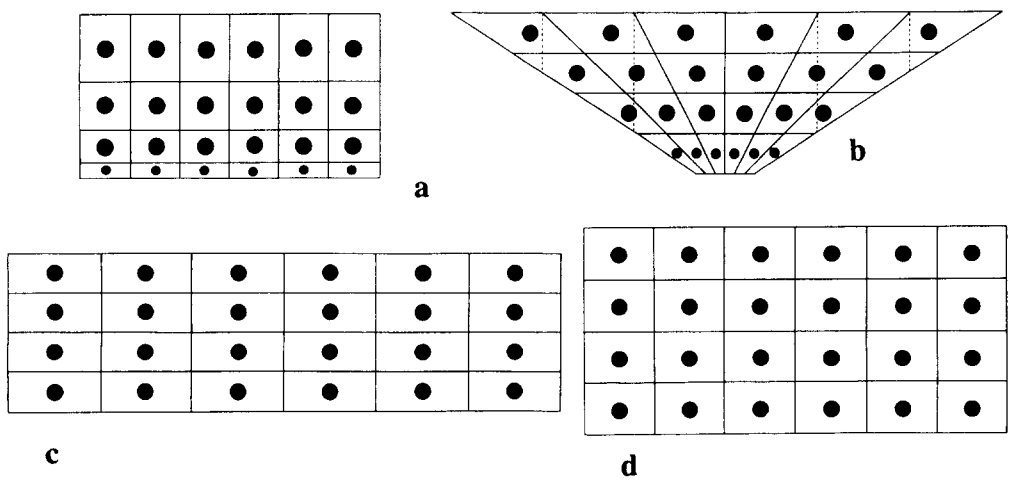

Fig. 4. Ideal fold shapes in Fig. 3 shown after removal of strain. There is no significance to the difference in size of the circular markers, this is just for convenience in representation. The spacing of the grid lines defines the differences among (a), (c) and (d). The homogeneous strain in (d), prior to the volume loss, is a pure shear.

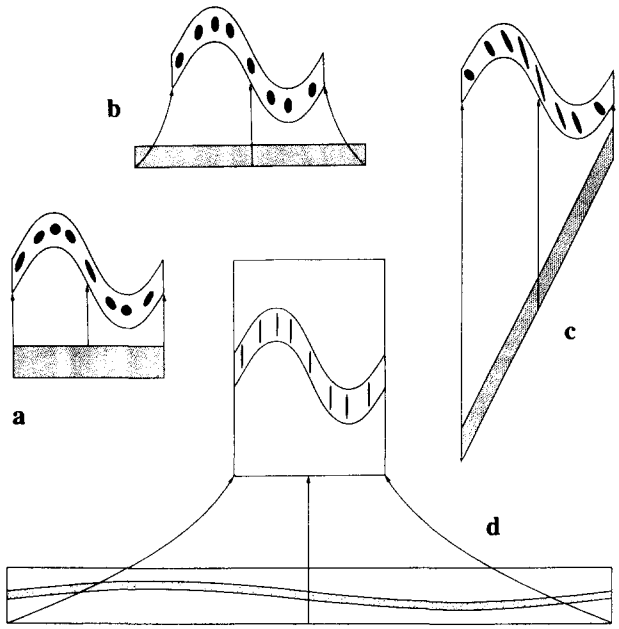

Fig. 5. Four different strain distributions in a similar fold produced by different combinations of simple shear and homogeneous strain. In (a)–(c) the initial layers are planar, in (d) an initial waviness exists. (a) Differential simple shear of alternating sense across the fold hinge—the 'classical' shear fold. (b) As in (a) with the simple shear preceded by homogeneous shortening. (c) Differential simple shear of the same sense throughout. (d) Homogeneous strain affecting original waviness in the layering. See Hudleston (1977) for discussion.

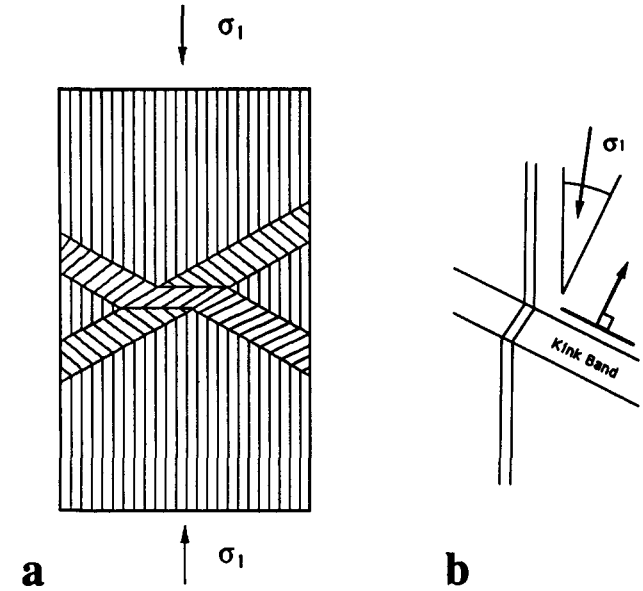

Fig. 6. Idealized kink bands, based on experimental work (e.g. Donath 1968), showing the relationship between the orientation of the maximum applied principal stress, σ_1, and the kink bands. (a) Conjugate kinks, for which σ_1 bisects the obtuse angle between the kink bands. (b) According to Donath (1968), σ_1 is contained in the angle between the foliation and the normal to the kink band, for a single set of kinks.

buckle if shortened and may develop pinch-and-swell or boudinage if extended, with little overall change in thickness or length. Reasonable estimates of shortening or extension parallel to the layer can be made by assuming the layer folds or pulls apart without change in length (e.g. Ramsay & Huber 1983, pp. 99–103, Ferguson 1987). Where there are buckled or boudinaged veins of many different orientations, Talbot (1970) has shown how information on the orientations of the principal strains and their axial ratios, for a three-dimensional state of strain, can be obtained. Measurement of strain using folds or boudins may lead to large underestimates because the stiff layer undergoes a certain amount of overall thickening or thinning before folds or boudins develop. Conversely, if folds are tight to isoclinal, an overestimation of strain is possible due to stretching of the fold limbs.

Interestingly, it is in principle possible to obtain information on both finite strain and vorticity (for *steady-state* homogeneous flow) using boudinaged and folded veins of various orientations to map out sectors of different history of shortening and elongation (Passchier 1990). This is a generalized treatment of the kind originally proposed by Ramsay (1967, figs. 3-62 and 3-64) to distinguish between simple shear and pure shear.

STRESS

In general nothing can be said from fold shape and orientation about the magnitudes and orientations of the regional principal stresses that produced folds, because folds are an integrated effect of the deformation. The principal directions of stress at any instant will not in general be parallel to the principal directions of cumulative strain. Information about principal stresses may be obtained, however, if strains are small, such as in the case of most kink bands (e.g. Fig. 2d), for which sense of offset on one or two sets allows the directions of the principal stresses to be estimated (Fig. 6) (Donath 1968). It has recently been shown (Williams & Price 1990) how kink bands are related to other band structures in foliated rocks in which the orientation of the principal stress to the foliation is systematically varied. In the experiments of Williams & Price, however, the deformation was quite ductile and fairly large non-coaxial strains (up to 25% shortening) were developed. It may prove possible, in a manner analogous to that demonstrated using twinning in calcite crystals (Jamison & Spang 1976), to use the intensity of kinking as some measure of stress magnitude. Finally, it may be possible to infer orientations of regional directions of principal stress from folds and other structures *if* it can be demonstrated that the bulk strain was coaxial or that a non-coaxial flow was steady-state (e.g. Weijermars 1991).

SENSE OF SHEAR

Fold asymmetry is readily established and can be used, with a few caveats, to deduce the sense of shear parallel to layering. Systematic asymmetry develops in parasitic folds on the limbs of larger folds (Fig. 7a), reflecting systematic variation in sense of shear around the larger fold. This property has long been used in identifying and mapping out large-scale folds using the practical and familiar designators of minor fold sym-

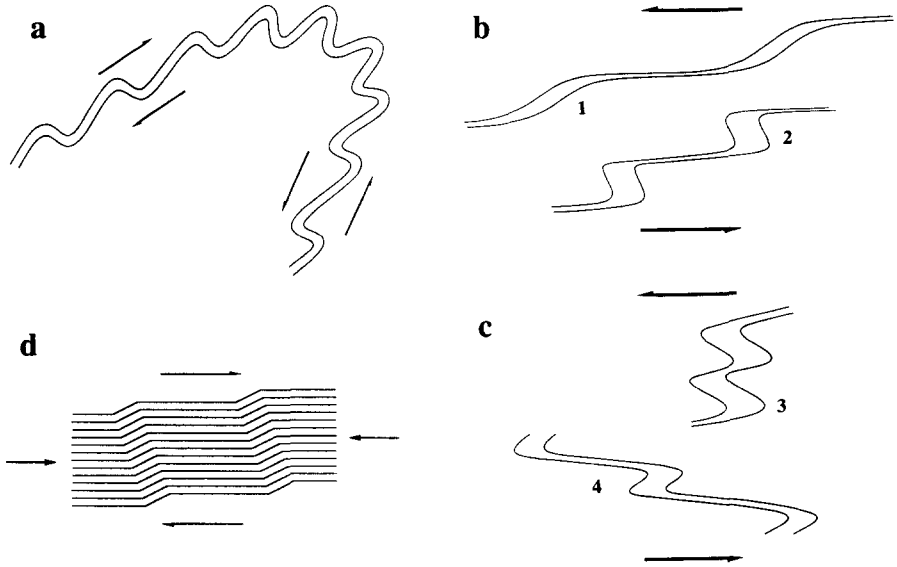

Fig. 7. Asymmetry of folds. (a) Parasitic folds around a larger fold displaying a systematic change in asymmetry from limb to limb reflecting local shear sense. Symmetry changes from Z on the left flank to M in the hinge and S on the right flank. (b) Passive folds developed in a shear zone. Amplification and the axial surfaces of the folds tend to be sub-parallel to the shear zone boundaries (see Hudleston 1977). (c) The example shown in (b) subjected to further shear, leading to a reversal in sense of asymmetry and a false indication of shear sense. (d) A kink fold developed under the stress conditions shown, with opposite sense of asymmetry to the resolved shear stress along the foliation (Reches & Johnson 1976).

metry S, Z and M. Systematic asymmetry also develops in layers inclined to the principal directions of bulk strain, and in ductile shear zones (Fig. 7b), in which fold initiation may be due to an instability (Ridley & Casey 1989) or passive (Hudleston 1977). It is nearly always consistent with the sense of shear. Problems may occur in shear zones in which strain is large, because sense of asymmetry may change with progressive strain as shown by Ramsay *et al.* (1983) for the lower limb of the Morcles nappe. This phenomenon is illustrated in Fig. 7(c). Also, in well-foliated rock in which shear strain is small, kinks may form antithetic to the direction of resolved shear stress (Fig. 7d) (Reches & Johnson 1976). Finally, local asymmetry may be inherited from the initial irregularities in the layer and have no bearing on layer-parallel shear (Abbassi & Mancktelow 1990, fig. 2b).

It should be pointed out that in any of the examples given above, asymmetric folds do not imply simple shear, they merely indicate, with the caveats noted, the sign of the shear strain associated with the general plane of layering.

RHEOLOGICAL PROPERTIES

Information about rheology can be gained by studies of the geometric characteristics of folds. Perhaps the simplest feature that can be used to determine relative viscosity across an interface (for pinch-and-swell and mullion structures as well as folds) is the tendency of the interface to take up a cuspate form, with the cusp always pointing toward the stiffer side of the interface (e.g. Figs. 1b & c). More information can be obtained by study of the wavelength/thickness, L/h, distributions of buckled (or extended by pinch-and-swell) isolated competent layers. For such studies, 'wavelength' is actually measured along the arc of mature folds (see Fig. 8). Buckling theory (Sherwin & Chapple 1968, Fletcher 1974, Smith 1975) predicts that a dominant value of wavelength/thickness, represented here by L_d, exists that depends on the ratio of viscosities of layer to matrix and the homogeneous shortening undergone by the layer. For materials of power-law type, appropriate for rocks deforming under natural conditions of crystal-plastic flow, L_d also depends on the exponent in the flow law (Fletcher 1974, Smith 1975, 1977). Smith shows that the theory applies to fluids of generalized non-linear rheology, not just power-law fluids.

Buckling is in fact just one of a related family of instabilities. Smith (1975, 1977) has developed the theory for all possible instabilities in a single embedded layer, stiffer or softer than its matrix and subjected to shortening or extension. A stiff layer under extension gives rise to a pinch-and-swell (or boudinage) instability, a soft layer in compression to mullion structure, and a soft layer in extension to inverse folding. All except buckling are weak instabilities, and only buckle folding is a strong instability in Newtonian materials. The existence of pinch-and-swell is by itself strong evidence for non-linear flow in the stiff layer, because in Newtonian fluids the dynamic pinch-and-swell instability is more than counteracted by kinematic damping. Mullions (in the sense of Smith 1975) are found in nature and have been produced experimentally (Sokoutis 1990). The existence of mullions is suggestive of non-linear flow because, even though the kinematic growth reinforces the dynamic instability, the instability is very weak in Newtonian materials. No convincing examples of natural inverse folding (the weakest of the instabilities) have been described. All four instabilities have the same dominant wavelength, for a given set of rheological parameters, but mature structures of the four types of

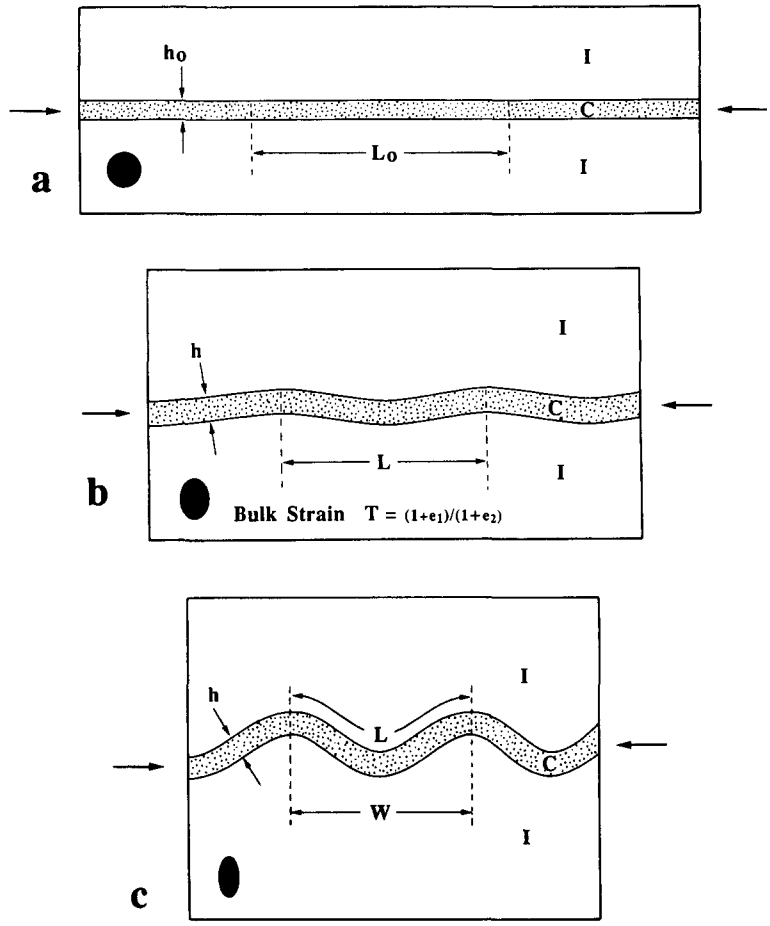

Fig. 8. Idealized stages of buckling of an isolated stiff layer (competent, C) in a soft matrix (incompetent, I) subjected to shortening in pure shear. (a) Initial state with layer of thickness h_0. L_0 is the length of the segment that will become one complete fold. (b) During the early stage of deformation and fold growth, the layer shortens and thickens almost uniformly to attain thickness h and length L, at a 'base flow' strain (homogeneous in layer and matrix) of $T = (1 + e_1)/(1 + e_2)$. At the end of this stage the folds have amplitudes of about 10–15°. True wavelength and L are almost equal throughout this stage. (c) During the later stage of buckling, the length and thickness of the stiff layer do not change significantly; they are in effect 'frozen in' at the end of the earlier stage. The arc length, L, during stage (c), not the wavelength, W, is the wavelength at the end of wavelength selection and is what is measured in order to estimate rheological parameters.

instability will have different values of preferred L/h because the shortening involved in each case to bring the structures to a given amplitude (say with dips of 10–15°) will differ significantly. An approximate expression (Fletcher 1974, Smith 1977) for the ratio of dominant wavelength to thickness (L_d) for both folding and boudinage at large values of viscosity ratio can be given:

$$L_d = 3.46 \frac{n_M^{1/6}}{n_L^{1/3}} m^{1/3}, \quad (1)$$

where $m = \mu_L/\mu_M$ is the ratio of viscosity of layer to viscosity of matrix in the steady flow on which the flow due to the instability is superimposed, and n_L and n_M are the exponents in the flow laws for layer and matrix. Note that shortening does not enter into this expression, and note also that perfect bonding between layer and matrix is assumed in the theoretical treatments of Fletcher (1974) and Smith (1975, 1977). Fletcher & Sherwin (1978) have shown that if the initial amplitude spectrum of the interface between stiff and soft layers is in the form of 'white roughness', the mean of the measured values of L/h is a good estimate of L_d for buckle folds.

There are other factors, notably strain softening (Neurath & Smith 1982) and layer anisotropy (Bayly 1970, Cobbold 1976, Casey & Huggenberger 1985), besides μ_L/μ_M and n that affect buckling instability (and thus L_d) and the shape of folds. There are thus too many unknowns to deduce rheological properties unambiguously from populations of natural folds (or the related structures pinch-and-swell and mullions), but if reasonable assumptions about the form of the initial wavelength spectra are made (Fletcher & Sherwin 1978), if strain in the competent layers can be measured independently, and if anisotropy is unimportant, estimates of rheological parameters, can be made (Fletcher 1974, Hudleston & Holst 1984, Hudleston & Tabor 1988). These include the value of power-law exponent n_L for the stiff layer (or effective power-law exponent if the flow is more complex (Smith 1977)) or if there is strain softening (Neurath & Smith 1982). An example of the L/h distribution for a natural fold population and the theoretical relationship among the parameters that can be measured or estimated for this population of folds are given in Fig. 9. Bearing in mind the simplifying assumptions made in applying the theory, these and other data (e.g. Fletcher 1974, Hudleston & Holst 1984, Hudleston

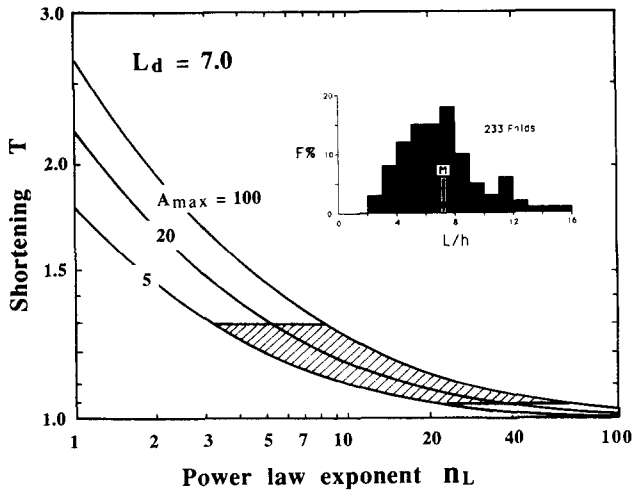

Fig. 9. Theoretical relationship (after Fletcher 1974) between 'shortening' expressed as the 'base flow' strain, T, and power-law exponent, n_L, of a stiff layer folded with a dominant wavelength given by $L_d = 7$, for various values of amplification of the dominant wavelength. The inset is a frequency distribution of arc length/thickness for a natural population of single-layer folds (calcite veins and limestone beds in slates) with a mean value, M, of about 7 (see Hudleston & Tabor 1988). Fletcher & Sherwin (1978) showed that the mean of such a distribution is a good estimate of the dominant wavelength/thickness if the initial irregularities in the layer have a spectrum of white roughness, as assumed here. For the natural folds, maximum amplification is estimated to be $5 < A_{max} < 100$ and strain in the layer to be $1.05 < T < 1.3$. These imply conditions for buckling to lie in the shaded area, and a value of power-law exponent for the stiff layer of $n_L \geq 3$. The upper limit of n_L is not well defined.

& Tabor 1988) are most consistent with non-linear constitutive relations for rocks in which natural folds have developed, although some fold data suggest linear behavior (Holst 1987). Smith (1979) has shown that for extremely non-linear flow, L_d will be in the range 4–6 regardless of viscosity ratio, and he argued that this is the reason why folds of such low values of L/h are so common in nature.

Information about rheology can also be gained from analyzing the shapes of individual folded surfaces of isolated buckled layers. This has the advantage that there is no need to estimate a dominant wavelength, the identification of which requires assumptions about the form of the initial amplitude spectra in the layers that are hard to test. It has the disadvantage, however, that there is quite a lot of 'noise' in fold shapes, reflecting some control of the irregularities in the initial shape on the final fold form, and thus requiring that a group of folds be analyzed in order to define a characteristic shape for a given set of conditions. Fold shapes can be studied using physical models or numerical models employing materials of known rheological properties. We have used the finite element method to do this, in which rheological properties and initial shapes can be precisely set (Lan & Hudleston 1991). We used a range of values of initial wavelength/thickness (L_o/h_o = 6–30) (set independently of the dominant wavelength), viscosity ratio in the unperturbed flow ($\mu_L/\mu_M = m$ = 10 and 100 for a linear stiff layer and higher values for non-linear stiff layers), and power-law exponent of the stiff layer (n_L = 1,3 and 10) likely to cover a broad range of values occurring in nature, and we kept the layer bonded to the matrix. The power-law exponent of the matrix was set $n_M = 1$. Varying n_M has significantly less effect on the instability than varying n_L, as can be shown if the rheological parameters are appropriately expressed (Fletcher 1974).

Strain gradient across a fold hinge and hinge thickening with respect to the limbs increase with fold growth. (Note that we use different symbols to represent 'bulk' strain, $T = (1+e_1)/(1+e_2)$, the homogeneous strain associated with the unperturbed base flow (Figs. 8 and 9) and strain, $R = (1+e_1)/(1+e_2)$, which is the total strain and is a function of position within the layer and matrix (Fig. 10). e_1 and e_2 are the principal extensions of either the bulk strain or the total strain.) At fixed amplitude or limb dip, both these quantities increase with increasing n_L. This is because the strain rate and strain increase more rapidly away from the neutral surface, on both sides, for a layer of power-law rheology (with $n_L > 1$) than for a layer of Newtonian rheology (Fig.10). The hinge is thicker because inner arc shortening thickens the layer more than outer arc extension thins it (Hudleston & Tabor 1988). Thus as n_L increases, strain is progressively concentrated in the hinge and the hinge thickens. The pattern of increase in hinge thickness with increasing fold amplitude differs in the linear and non-linear cases, with most thickening in the linear case occurring late in fold development, and most thickening in the non-linear case occurring early in fold development. This is discussed in Lan & Hudleston (in preparation). By comparing strain gradients in folds of simi-

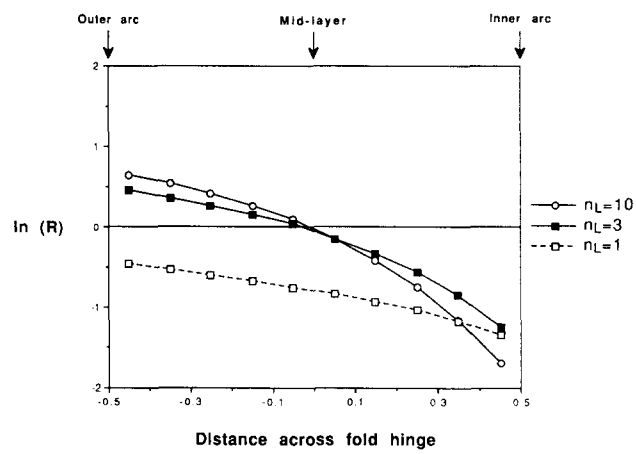

Fig. 10. Natural logarithm of strain ratio, R, plotted against normalized distance across the hinge of three simulated buckle folds, with the same initial wavelength/thickness (L_o/h_o = 12), and amount of bulk shortening imposed (S = 40%), but with different values of power-law exponent, n_L, of the stiff layer. The viscosity ratio, m, in the base flow is 10, 215 and 630, respectively, for n_L = 1, 3 and 10. $R = (1 + e_1)/(1 + e_2)$ or $(1 + e_2)/(1 + e_1)$ depending on which principal strain is parallel to the layer. Note the difference in strain gradient in the three cases, the highest gradient associated with the highest values of n_L. Also note the existence of a neutral surface for n_L = 3 and 10, given by the point ln R = 0, but not for n_L = 1. This reflects the strong effect of early layer-parallel shortening for n_L = 1 and the fact that the buckling instability in this case is weak. The effect of this uniform layer-parallel shortening could be removed from the strains associated with the folding by moving the curve for n_L = 1 vertically downwards. Note the distinction between R, the total strain varying as a function of position in the layer, and T (Figs. 8 and 9), the homogeneous strain on which the buckling strains are superimposed.

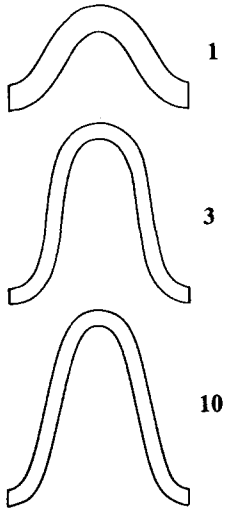

Fig. 11. The shapes of mature folds produced in computer simulations, under plane strain and bulk pure shear, for starting configurations $A_o/h_o = 0.1$ and $L_o/h_o = 30$ in all cases, and for $n_L = 1, 3$ and 10, and $m = 1, 215$ and 630, respectively.

lar amplitude and L/h, it should be possible to distinguish highly non-linear stiff layer behavior from linear behavior.

Curvature analysis

Hinge-thickening is related to overall fold shape. The hinges become sharper as n_L increases and the limbs become relatively longer and straighter. Examples of this are shown in Fig. 11 for folds developed from an identical initial configuration (sinusoidal shape, with amplitude/h_o = 0.1, and L_o/h_o = 30) after 60% bulk shortening. The overall differences in shape with increasing n_L are apparent in Fig. 11 and even more so in plots of curvature as a function as distance across the fold (Fig. 12). There is a gradual decrease in curvature away from the outer arc hinge for $n_L = 1$, and a smooth transition through the inflexion point. This contrasts with a rapid decrease in curvature away from the outer arc hinge for $n_L = 10$ and a section of almost straight limb around the inflection point, reflecting a concentration of strain in the hinge region. The curvature variations for $n_L = 3$ are intermediate between those for $n_L = 1$ and $n_L = 10$. The essence of these differences can be expressed using a curvature index, k_i, which is defined (work in preparation) as the ratio of the distance between the inflexion point (where curvature is zero) and the point at which curvature attains 0.75 of its maximum value to the distance between the inflexion point and the hinge (where curvature is maximum). Distances are measured from the inflexion point to the projections of the points at which $k = 0.75\ k_{max}$ and $k = k_{max}$ (hinge) on an axis (x-co-ordinate in Fig. 12) through the inflexion point and perpendicular to the axial plane. The index, k_i, has a value of 1 for a chevron or zig-zag fold, 0 for a fold formed by circular arcs, and 0.77 for a sine wave. We have interpolated the results of many computer simulations to arrive at plots of k_i vs limb dip for constant L/h (not constant L_o/h_o, note) and k_i vs L/h for constant limb dip. Examples are shown in Fig. 13. Our results show that k_i increases with both L/h

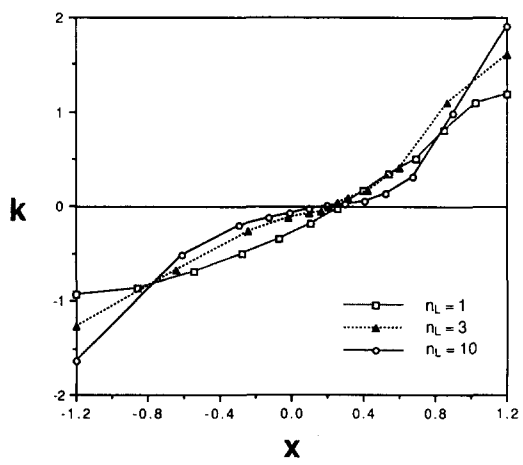

Fig. 12. Curvature, k, for the folds shown in Fig. 11, as a function of co-ordinate distance, x, from 'anticlinal' hinge or outer arc (left) to 'synclinal' hinge or inner arc (right). Note the increased length of the zone of low values of k (say $|k| < 0.25$) around the inflexion point as n_L is increased.

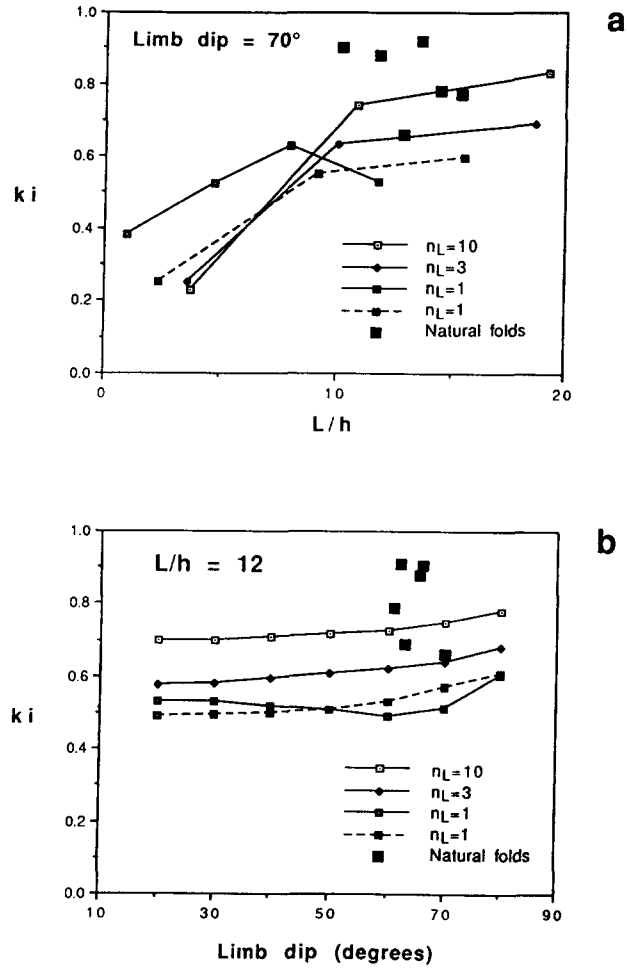

Fig. 13. Curvature index, k_i, as a function of L/h (a) and limb dip (b) for buckle folds interpolated from results of numerical models with different values of n_L for the stiff layer, and data for a population of natural folds in siltstone layers in shales from the central Appalachians. Numerical results shown as solid lines are for $n_L = 1, 3$ and 10 and viscosity ratio $m = 10, 215$ and 630 respectively. Increasing m by an order of magnitude ($m = 100, 2100$ and 6300) gives results similar to those plotted (except for $n_L = 1$), and the results are only shown for $n_L = 1$, which is represented by a dashed line.

and limb dip, but that the increases with L/h (Fig. 13a) and with limb dip (Fig. 13b) at $L/h > 10$ are modest. They also show a dependence of k_i on n_L that is well-defined for $L/h > 10$. Data for experimentally-produced folds, for which rheological properties are reasonably well known, are consistent with these results (Fig. 13) (work in preparation). Our results also show that k_i (but not, one should note, L_d) is relatively insensitive to changes in m. Changing m by an order of magnitude does not significantly affect the value of k_i, except for the case of $n_L = 1$ (Fig. 13).

If we are to use curvature variations to deduce rheological properties of folded layers, we need to be able to assess the effect of variations in the initial shapes of folds (i.e. in irregularities in the layering) on the final fold shapes observed. We have done this in our computer simulations by using several very different shapes of low amplitude (work in preparation). We find that for strong buckling instabilities ($n_L \geq 3$, $m \geq 200$) the final fold shape is almost independent of initial shape. For $n_L = 1$ and $m = 10$, representing a weak buckling instability, there is a modest dependence of final shape on initial shape preserved at high amplitudes. These simulations indicate that fold shape should indeed preserve information on rheological state.

Limb dip, k_i and L/h can all be measured readily on natural folds and provide a basis for fold interpretation in light of the numerical results. Data for some natural folds are plotted in Fig. 13. They are not consistent with linear rheological behavior and, in fact, they lie in the field of very high values of n_L, suggesting that other factors, such as plastic yield (Chapple 1969), strain softening (see Neurath & Smith 1982) or anisotropy (Cobbold 1976), may be influencing fold shape, all of which may lead to increased sharpness of folds. The presence of strong crystallographic preferred orientations or shape fabrics (particularly of phyllosilicates) in many natural folds suggests that anisotropy is probably significant (e.g. Bayly 1969). Cobbold (1976) has argued that a planar anisotropy can lead to instabilities and growth of sharp-hinged folds (which would have high values of k_i) and Ridley & Casey (1989) have demonstrated this effect very nicely for folds developed in anisotropic materials in shear zones. This is a subject that merits further investigation.

CONCLUSIONS

The state of strain in rocks cannot be inferred from fold shapes alone, although fold shapes do provide some constraints on possible strain distributions, especially if additional originally planar or linear markers are present. Except in a few special circumstances, fold asymmetry reflects the sense of shear strain parallel to the general orientation of the folded layering, and thus is a useful sense-of-shear indicator. Information on the orientation of 'bulk flow' principal stresses cannot be obtained from folds, unless the strain is small and the mechanism of folding understood, as for kink bands, or unless it can be demonstrated that the bulk strain is coaxial.

Some information on rheological properties of rocks at the time of folding can be obtained from a study of the distribution of wavelength/thickness in fold populations and the pattern of curvature variation in individual single-layer folds. Although non-unique and with significant uncertainty attached, such information complements information obtained from experimental rock deformation (e.g. Kirby & Kronenberg 1987) and analysis of microfabric that allows identification of probable deformation mechanisms and thus possible flow laws (e.g. Schmid 1982). From the limited data now available, there seems to be mutual consistency among these different approaches.

Acknowledgements—Through his publications, lectures and field trips, John Ramsay has been a source of inspiration to one of us (P. J. Hudleston) for many years. He has showed just how much could be learned about deformation of rocks by a careful study of the shapes and attitudes of folds and the fabrics within them. His work on the topic is seminal. Part of the research described in this paper was supported by grants from the National Science Foundation (EAR-8804670) and the University of Minnesota Supercomputer Institute. This support is gratefully acknowledged. The manuscript has benefitted from reviews by John Cosgrove and an anonymous person.

REFERENCES

Abbassi, M. R. & Mancktelow, N. S. 1990. The effect of initial perturbation shape and symmetry on fold development. *J. Struct. Geol.* **12**, 279–282.

Bayly, M. B. 1969. Anisotropy of viscosity in suspensions of parallel flakes. *J. Composite Materials* **3**, 705–708.

Bayly, M. B. 1970. Viscosity and anisotropy estimates from measurements on chevron folds. *Tectonophysics* **9**, 459–474.

Billings, M. P. 1972. *Structural Geology* (3rd edn). Prentice-Hall, Englewood Cliffs, New Jersey.

Borradaile, G. J. 1978. Transected folds: a study illustrated with examples from Canada and Scotland. *Bull. geol. Soc. Am.* **89**, 481–493.

Busk, H. G. 1929. *Earth Flexures*. Cambridge University Press, Cambridge.

Carey, S. W. 1962. Folding. *J. Alberta Soc. Petrol. Geol.* **10**, 95–144.

Casey, M. & Huggenberger, P. 1985. Numerical modelling of finite-amplitude similar folds developed under general deformation histories. *J. Struct. Geol.* **7**, 103–114.

Chapple, W. M. 1969. Fold shape and rheology: the folding of an isolated viscous-plastic layer. *Tectonophysics* **7**, 79–116.

Cobbold, P. R. 1976. Mechanical effect of anisotropy during large finite deformation. *Bull. Soc. géol. Fr.*, 7 *Sér.* **18**, 1497–1510.

Donath, F. A. 1968. The development of kink bands in brittle anisotropic rock. *Mem. geol. Soc. Am.* **115**, 453–493.

Elliott, D. 1965. The quantitative mapping of directional minor structures. *J. Geol.* **73**, 865–880.

Ferguson, C. C. 1987. Fracture and separation histories of stretched belemnites and other rigid–brittle inclusions in tectonites. *Tectonophysics* **139**, 255–273.

Fleuty, M. J. 1964. The description of folds. *Proc. Geol. Ass.* **75**, 461–492.

Fletcher, R. C. 1974. Wavelength selection in the folding of a single layer with power-law rheology. *Am. J. Sci.* **274**, 1029–1043.

Fletcher, R. C. & Sherwin, J. 1978. Arc lengths of single layer folds: a discussion of the comparison between theory and observation. *Am. J. Sci.* **278**, 1085–1098.

Flinn, D. 1962. On folding in three-dimensional progressive deformation. *Q. Jl geol. Soc. Lond.* **118**, 385–433.

Hobbs, B. E. 1972. Deformation of non-Newtonian materials in simple shear. In: *Flow and Fracture of Rocks* (edited by Heard, H. C., Borg, I. Y., Carter, N. L. & Raleigh, B. C.). *Am. Geophys. Un. Geophys. Monogr.* **16**, 243–258.

Holst, T. B. 1987. Analysis of buckle folds from the early Proterozoic of Minnesota. *Am. J. Sci.* **287**, 612–634.

Hudleston, P. J. 1973. Fold morphology and some geometrical implications of theories of fold development. *Tectonophysics* **16**, 1–46.

Hudleston, P. J. 1977. Similar folds, recumbent folds, and gravity tectonics in ice and rocks. *J. Geol.* **85**, 113–122.

Hudleston, P. J. & Holst, T. B. 1984. Strain analysis and fold shape in a limestone layer and implications for layer rheology. *Tectonophysics* **106**, 321–347.

Hudleston, P. J. & Tabor, J. R. 1988. Strain and fabric development in a buckled calcite vein. *Bull. Geol. Inst., Univ. Uppsala N.S.* **14**, 79–94.

Jamison, W. R. & Spang, J. H. 1976. Use of calcite twin lamellae to infer differential stresses. *Bull. geol. Soc. Am.* **87**, 868–872.

Johnson, T. E. 1991. Nomenclature and geometrical classification of cleavage-transected folds. *J. Struct. Geol.* **13**, 261–274.

Kirby, S. H. & Kronenberg, A. K. 1987. Rheology of the lithosphere: selected topics. *Rev. Geophys.* **23**, 1219–1244.

Lan, L. & Hudleston, P. J. 1991. Numerical models of buckle folds in non-linear materials. *Tectonophysics* **199**, 1–12.

Manz, R. & Wickham, J. 1978. Experimental analysis of folding in simple shear. *Tectonophysics* **44**, 79–90.

Mertie, J. B. 1959. Classification, delineation and measurement of non-parallel folds. *Prof. Pap. U.S. geol. Surv.* **314E**, 91–124.

Neurath, C. & Smith, R. B. 1982. The effect of material properties on growth rates of folding and boudinage: experiments with wax models. *J. Struct. Geol.* **4**, 215–229.

Passchier, C. 1990. Reconstruction of deformation and flow parameters from deformed vein sets. *Tectonophysics* **180**, 185–199.

Ragan, D. M. 1969. Structures at the base of an ice fall. *J. Geol.* **77**, 647–667.

Ramberg, H. 1963. Strain distribution and geometry of folds. *Bull. Geol. Inst., Univ. Uppsala* **42**, 1–20.

Ramsay, J. G. 1962. The geometry and mechanism of formation of similar folds. *J. Geol.* **70**, 309–327.

Ramsay, J. G. 1967. *Folding and Fracturing of Rocks*. McGraw-Hill, New York.

Ramsay, J. G., Casey, M. & Kligfield, R. 1983. Role of shear in development of the Helvetic fold-thrust belt of Switzerland. *Geology* **11**, 439–442.

Ramsay, J. G. & Huber, M. I. 1983. *The Techniques of Modern Structural Geology, Volume* 1: *Strain Analysis*. Academic Press, London.

Ramsay, J. G. & Huber, M. I. 1987. *The Techniques of Modern Structural Geology, Volume* 2: *Folds and Fractures*. Academic Press, London.

Reches, Z. & Johnson, A. M. 1976. A theory of concentric, kink and sinusoidal folding and of monoclinal flexuring of compressible, elastic multilayers: VI, Asymmetric folding and monoclinal kinks. *Tectonophysics* **35**, 295–334.

Ridley, J. & Casey, M. 1989. Numerical modeling of folding in rotational strain histories: strain regimes expected in thrust belts and shear zones. *Geology* **17**, 875–878.

Schmid, S. M. 1982. Microfabric studies as indicators of deformation mechanisms and flow laws operative in mountain building. In: *Mountain Building Processes* (edited by Hsü, K. J.). Academic Press, New York, 95–110.

Sherwin, J. & Chapple, W. M. 1968. Wavelengths of single layer folds: a comparison between theory and observation. *Am. J. Sci.* **266**, 167–179.

Smith, R. B. 1975. Unified theory of the onset of folding, boudinage, and mullion structure. *Bull. geol. Soc. Am.* **86**, 1601–1609.

Smith, R. B. 1977. Formation of folds, boudinage, and mullions in non-Newtonian materials. *Bull. geol. Soc. Am.* **88**, 312–320.

Smith, R. B. 1979. The folding of a strongly non-Newtonian layer. *Am. J. Sci.* **279**, 272–287.

Sokoutis, D. 1990. Experimental mullions at single and double interfaces. *J. Struct. Geol.* **12**, 365–373.

Stabler, C. L. 1968. Simplified Fourier analysis of fold shapes. *Tectonophysics* **6**, 343–350.

Talbot, C. J. 1970. The minimum strain ellipsoid using deformed quartz veins. *Tectonophysics* **9**, 47–67.

Thiessen, R. L. 1986. Two-dimensional refold interference patterns. *J. Struct. Geol.* **8**, 563–573.

Treagus, S. H. 1973. Buckling instability of a viscous single-layer system, oblique to the principal compression. *Tectonophysics* **19**, 271–289.

Twiss, R. J. 1988. Description and classification of folds in single surfaces. *J. Struct. Geol.* **10**, 607–623.

Van Hise, C. R. 1896. Principles of North American Pre-cambrian Geology. *U.S. geol. Surv. Ann. Rep.* **16**, 571–843.

Weijermars, R. 1991. The role of stress in ductile deformation. *J. Struct. Geol.* **13**, 1061–1078.

Weiss, L. E. 1972. *The Minor Structures of Deformed Rocks: A Photographic Atlas*. Springer, New York.

Williams, P. F. & Price, G. 1990. Origin of kinkbands and shear band cleavage in shear zones: an experimental study. *J. Struct. Geol.* **13**, 145–164.

Wilson, G. 1967. The geometry of cylindrical and conical folds. *Proc. Geol. Ass.* **78**, 179–200.